Letter

Structural phase transition involving octahedron tilting and ion migration in metal-halide perovskites: A machine-learning study

Xinjian Ouyang,[1,2] Weijia Chen,[1,2] Yanxing Zhang,[3] Feng Zhang,[1,2] Yuan Zhuang,[1,2] Xiao Jie,[1,2] Laijun Liu,[4] and Dawei Wang[1,2,*]

[1]*School of Microelectronics & State Key Laboratory for Mechanical Behavior of Materials, Xi'an Jiaotong University, Xi'an 710049, China*

[2]*Key Lab of Micro-Nano Electronics and System Integration of Xi'an City, Xi'an Jiaotong University, Xi'an 710049, China*

[3]*School of Physics, Henan Normal University, Xinxiang 453007, China*

[4]*Key Laboratory of Nonferrous Materials and New Processing Technology, Ministry of Education, College of Materials Science and Engineering, Guilin University of Technology, Guilin, 541004, China*

(Received 14 May 2023; accepted 14 July 2023; published 28 July 2023)

Metal-halide perovskites exhibit excellent optoelectronic properties, making them suitable for various applications. In this work, we propose a novel approach, employing the message-passing neural networks (MPNNs), to model the potential energy surface (PES) of metal-halide perovskites. The MPNN model can learn the PES of perovskites with an error of less than 1 meV per atom, which is comparable to *ab initio* calculations. With the accurate and fast prediction of the MPNN model, we perform large-scale molecular dynamics simulations for $CsPbBr_3$ and $Cs_2AgBiBr_6$, successfully identifying their temperature-dependent octahedron tilting patterns, ion displacement, and structural phases that are crucial to obtaining their electronic structure correctly. We also observe significant Ag migration and vacancy defects in $Cs_2AgBiBr_6$, which are further investigated using *ab initio* calculations, offering insights into its ambient stability. This work provides a comprehensive understanding of the structural phase transition in metal-halide perovskites, as well as information regarding ion migration.

DOI: 10.1103/PhysRevB.108.L020103

In recent years, metal-halide perovskites have gained much attention due to their fascinating photovoltaic properties and promising applications in solar cells and light emitting devices [1–4]. For these applications, it is important to know their stable phases at room temperature since different structural phases have very different band gap that can strongly affect their optical properties [5–7]. Moreover, it is also important to understand the degradation pathway and ambient stability of halide perovskites, which are usually related to ion migrations [8–11]. Common *ab initio* calculation often has difficulties to handle such requirements.

To obtain the temperature-dependent properties of perovskites, such as their structural phases and other dynamic properties, the effective Hamiltonian [12,13] and the core-shell model [14–16] are two popular methods, which derive the potential energy surface (PES) in a model-driven way by splitting the total energy into multiple terms with dozens of parameters, which are then fitted using *ab initio* calculations. The parameter fitting procedure typically requires additional human effort. Another two difficulties, including the strong anharmonic PES of metal-halide perovskites [17–19] and the small energy signature associated with octahedron tilting [20], hinder the investigation of halide perovskites. As a matter of fact, there are few investigations on the structural phase transitions of halide perovskites, except for the notable work on $CsPbI_3$ [21]. The investigation of double halide perovskites, or more complex systems, is essentially nonexistent. This work will address the paucity of numerical simulations on halide perovskites through a data-driven machine-learning-based approach.

The recent advancement of machine-learning potential models [22–28] has provided new opportunities to construct the PES for a given system and investigate its structural changes. A representative work is the investigation of methylammoniumPb_3 using Gaussian approximation potential [29]. Here, we propose to use message-passing neural networks (MPNNs) [30–33] to derive the highly anharmonic PES of metal-halide perovskites. As neural network models, MPNNs can in principle approximate any function upon proper data sets [34,35], where the parameters are optimized automatically during the training process, eliminating the need for human intervention. An MPNN model represents the chemical structure as an indirect graph, in which nodes (edges) correspond to atoms (interacting atom pairs). MPNN also includes the message-passing scheme, playing a central role in learning the interaction between atoms [36].

In this Letter, we present an MPNN-based molecular dynamics (MD) approach and study two specific halide perovskites, namely $CsPbBr_3$ and $Cs_2AgBiBr_6$. $CsPbBr_3$ is an attractive candidate for photovoltaic devices due to its high power conversion efficiency and long carrier lifetime [37,38], while $Cs_2AgBiBr_6$ is an environment-friendly double halide perovskite compared to $CsPbB_3$, as Pb cations are replaced by alternating Ag and Bi cations with the rock-salt ordering [39]. In this work, we will explore the octahedron tilting phase

*dawei.wang@xjtu.edu.cn

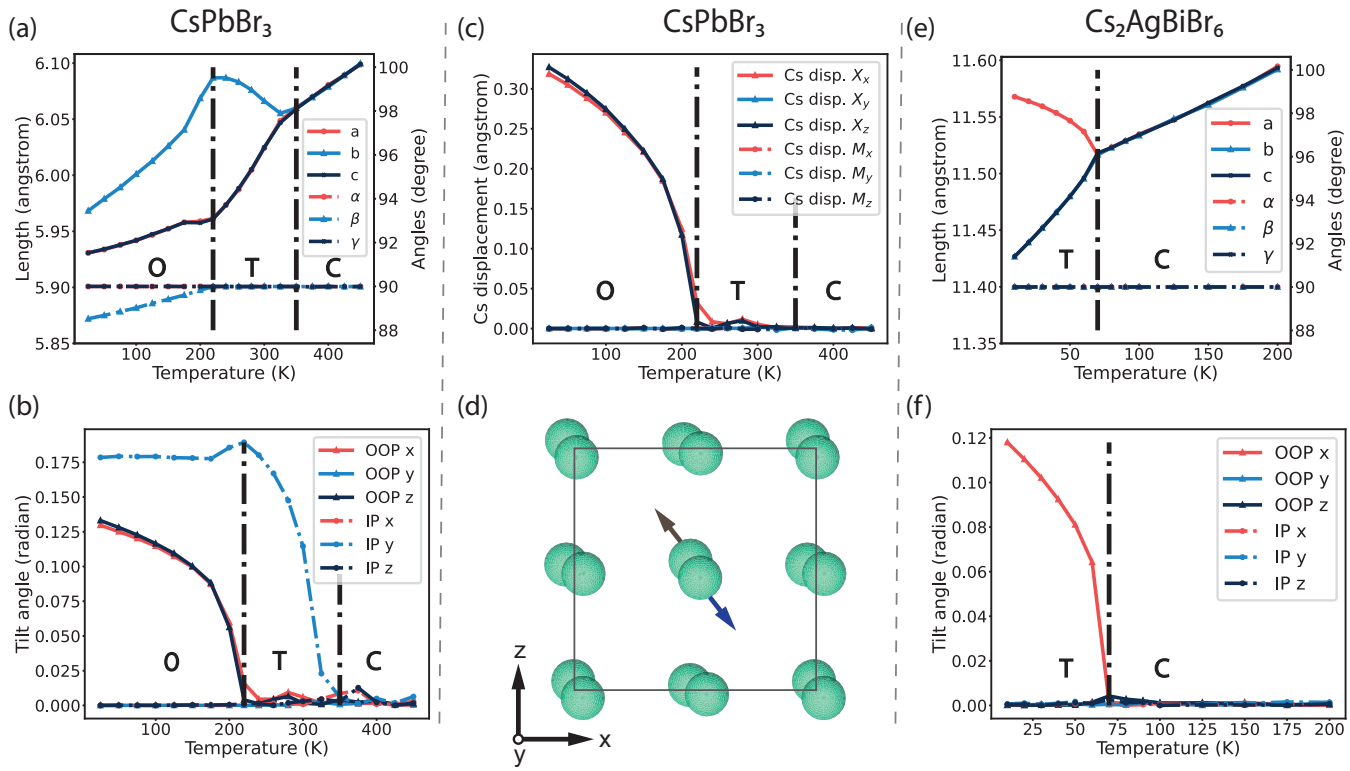

FIG. 1. The simulated temperature-dependent cubic-tetragonal-orthorhombic (C-T-O) phase transition of bulk $12 \times 12 \times 12$ $CsPbBr_3$ (a)–(d) and the cubic-tetragonal phase transition of bulk $6 \times 6 \times 6$ $Cs_2AgBiBr_6$ (e), (f). (a), (e) The lattice parameters of $CsPbBr_6$ and $Cs_2AgBiBr_6$; (b), (f) The octahedron tilt angles of $CsPbBr_3$ and $Cs_2AgBiBr_6$ in in-phase (IP) mode and out-of-phase (OOP) mode; (c) The absolute average displacement of Cs ions relative to the cubic state; (d) The Cs displacement projected in the x-z plane at 25 K, showing the antiferroeletrics of orthorhombic phase for $CsPbBr_3$. For sake of clarity, only a $2 \times 2 \times 2$ cell is drawn in (d), where the brown and blue arrows represent opposite displacement of Cs ions in alternating x-z planes. The vertical dotted line indicates the estimated phase transition temperature.

transitions in the two compounds, and discuss the Ag migration observed in $Cs_2AgBiBr_6$. By comparing the results to experiments [40–43], we demonstrate the potential of MPNNs in large-scale simulations of metal-halide perovskites. The MPNN model acts as an energy calculator in MD simulation, which takes the structural geometry and atomic numbers as inputs, outputs energy, and derives force and stress tensor by autodifferentiation [44] of the neural networks. A general MPNN framework follows the process of graph representation, message embedding, message interaction and the final property readout. The messages usually encode structural information, such as the relative distance between two atoms and their atomic numbers. Additionally, the angular information is added into the messages as they pass along the neural network, which represents three-body interactions and makes the model more sensitive to the spatial displacement of atoms [45]. The computational time complexity of MPNNs is $O(N)$ within the locality assumption [26], which scales linearly with the size of system and allows for fast prediction. The MPNN we employ is the DimeNet++ [32,33], which is adapted to periodic crystals with some modifications, and the loss function is designed in a physics-informed way by including physical inductive biases [46]. Further details on the MPNN and the loss function are available in Supplemental Material (SM) [47] Sec. I.

We perform a series of *ab initio* MD simulations to generate samples before training MPNN models. The density functional theory (DFT) calculations are based on the projector-augmented wave (PAW) [48,49] method, implemented in the GPAW [50] and ASE [51]. Specifically, the DFT calculations use a $2 \times 2 \times 2$ supercell for $CsPbBr_3$ and a $1 \times 1 \times 1$ unit cell for $Cs_2AgBiBr_6$ (both containing 40 atoms), the Perdew-Burke-Ernzerhof (PBE) [52] exchange-correlation functional, plane waves with a cutoff energy of 900 eV, and a $3 \times 3 \times 3$ k-point mesh. MD simulations are carried out in the NPT (constant particle number, pressure, and temperature) ensemble, using Nose-Hoover dynamics [53,54] to control the temperature and pressure.

To investigate the octahedron tilting phase transition in $CsPbBr_3$ and $Cs_2AgBiBr_6$, we start by training MPNN models using the generated data sets. The accuracy of the trained MPNN models is presented in SM [47] Sec. II. With the well-trained MPNN model providing energy, force, and stress, we then carry out NPT-MD simulations, where the external pressure is set as zero, the time step is 2 fs, and the number of simulation steps for each temperature is 50 000 (100 ps) for $CsPbBr_3$ and 100 000 (200 ps) for $Cs_2AgBiBr_6$, of which the last quarter are used to average order parameters. The simulation starts from a structure of $12 \times 12 \times 12$ five-atom cubic cells and a sufficiently high temperature, which gradually decreases to near 0 K. We first show the simulated phase transitions of $CsPbBr_3$ in Figs. 1(a)–1(d). For accurate description, the phase transition is analyzed in two aspects, i.e., structural distortions and octahedron tilting modes, which

are, respectively, described by the lattice parameters of the system and quantified by the R and M Brillouin points average that are characterized by different wave vectors $\boldsymbol{q}$ [55]. More precisely, the R-point average corresponds to the out-of-phase (OOP) tilts with $\boldsymbol{q}_R = (2\pi/a)(1/2, 1/2, 1/2)$ and the M-point averages correspond to in-phase (IP) tilts with $\boldsymbol{q}_{M_x} = (2\pi/a)(0, 1/2, 1/2)$, $\boldsymbol{q}_{M_y} = (2\pi/a)(1/2, 0, 1/2)$ and $\boldsymbol{q}_{M_z} = (2\pi/a)(1/2, 1/2, 0)$ around three axes, respectively, where a is the pseudocubic unit cell constant. The tilting modes are determined by considering each ABX_3 pseudocubic cell, where the tilt angle is calculated using the three B-X bonds without considering octahedron distortions. For convenience, the octahedron tilting modes are denoted by Glazer's notation [56].

Figures 1(a) and 1(b) show the lattice parameters and $PbBr_6$ octahedron tilting modes of $CsPbBr_3$ as a function of temperature, clearly revealing the existence of three phases. Above 350 K, $CsPbBr_3$ adopts the $Pm\bar{3}m$ cubic phase, where $a = b = c$ that decreases with temperature, and $\alpha = \beta = \gamma = 90^\circ$. In addition, Fig. 1(b) indicates that no octahedron tilt occurs in cubic phase, with the average tilting pattern being $a^0a^0a^0$. In the temperature range between 220 K and 350 K, the lattice parameters indicate the $P4/mbm$ tetragonal phase, where the crystal stretches along the y axis, and only the IP tilts around the y axis are present, leading to a $a^0b^+a^0$ tilting pattern with the maximum tilting angles of 0.186 radians (10.66°) at 220 K. Below 220 K, the angle between b and c starts to shrink until it reaches 88.5° at the lowest temperature 25 K, and the tilts add OOP modes around the x and z axes with a same angle of 0.130 radians (7.45°), indicating the $Pnma$ orthorhombic phase with an $a^-b^+a^-$ tilting pattern.

The displacement of Cs ions is a crucial factor in the tetragonal-orthorhombic transition and usually associated with the polarization of the system [57]. Figure 1(c) shows the average displacement of Cs ions through X and M points analysis. The X point [$\boldsymbol{q}_X = (2\pi/a)(0, 1/2, 0)$] analysis indicates that, below 220 K (the orthorhombic phase), the Cs ions shifts equally on average along the x and z direction ($X_x = X_z > 0$). Meanwhile, the M-points analysis reveals that the displacement of Cs in the neighboring x-z planes is equal but in opposite directions, resulting in a total displacement of zero ($M_x = M_z = 0$). The displacement of Cs at 25 K is schematically shown in Fig. 1(d). Above 220 K, the average displacement of Cs ions is zero in terms of both X and M points. Hence, we confirm the antiferroelectric nature of the low-temperature $Pnma$ phase.

All things considered, Figs. 1(a)–1(d) reveal that $CsPbBr_3$ undergoes cubic-tetragonal-orthorhombic (C-T-O) phase transitions as the temperature decreases, in good agreement with reported experiments [41–43]. Particularly, the change of lattice parameters closely resembles experimental results (Fig. 7 in Ref. [43]). However, the simulated phase transition temperatures are lower than the experimental values, with 350 K and 220 K for C-T and T-O transitions, respectively, compared to 403 K and 361 K for the same transitions reported in Ref. [42]. This discrepancy is a known issue that arises from the choice of the exchange-correlation function, which poses a challenge to DFT calculations [58,59].

We note that You *et al.* [60] recently investigated the temperature dependence of $CsPbBr_3$'s structural and thermal properties using the bond-valence model [61,62]. A detailed

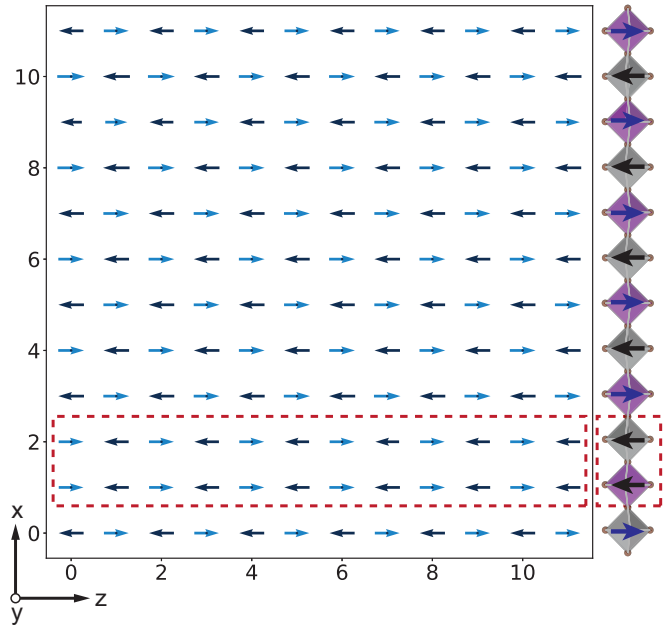

FIG. 2. Domain walls formed by the coexistence of $a^-b^0b^0$ and $a^+b^0b^0$ tilts for the bulk $6 \times 6 \times 6$ $Cs_2AgBiBr_6$ at 25 K, viewed from y direction for some x-z plane, where the blue and black arrows indicate opposite tilting directions. The right panel shows the alternate $BiBr_6$ (pink) and $AgBr_6$ (gray) octahedra (along three directions) in the $Cs_2AgBiBr_6$ network, with arrows showing tilting directions.

comparison between our work and theirs can be found in Sec. III of the SM [47]. We also note that one experiment [63] reports a possible $Cmcm$ phase in $CsPbBr_3$, which, according to the tilting pattern of $Cmcm$ phase [55,64], was not observed in our simulation. While $CsPbBr_3$ contains the toxic element lead, $Cs_2AgBiBr_6$ is a benign alternative to $CsPbBr_3$ with favorable band gap [65]. Figures 1(e) and 1(f) present the simulated phase transition of $Cs_2AgBiBr_6$. Above 70 K, the system is in a tiltless $a^0a^0a^0$ cubic state, around 70 K, the C-T phase transition occurs, and below 70 K $Cs_2AgBiBr_6$ remains in an $a^-b^0b^0$ tilting tetragonal phase, with the tilting angle reaching 0.118 radians (6.76°) at 10 K. The simulated phase transition temperature is close to the experimental values of 122 K [40]. We note that the double potential well of $Cs_2AgBiBr_6$ relating to tilts is as shallow as 0.5 meV per atom [see Fig. S3(b)], which requires a significant accuracy from the MPNN model to capture. We investigate the displacement of Cs in $Cs_2AgBiBr_6$ in a similar manner to $CsPbBr_3$, and find no average Cs displacement, resulting in the $I4/m$ tetragonal phase, which corresponds to the $I4/mcm$ tetragonal phase of single-halide perovskites [39]. In general, the phase transitions produced by the MPNN-based MD approach agree well with experiments, even for the complex double perovskite $Cs_2AgBiBr_6$ with small tilting energy signature.

Interestingly, during the simulation of $Cs_2AgBiBr_6$, we sometimes observe domains resulting from the coexistence of $a^-b^0b^0$ and $a^+b^0b^0$ tilts around the x axis, as shown in Fig. 2, in which the two red dotted boxes indicate where the $a^+b^0b^0$ tilts occur. We find that the emerging domains and domain walls are a metastable state. For instance, domains

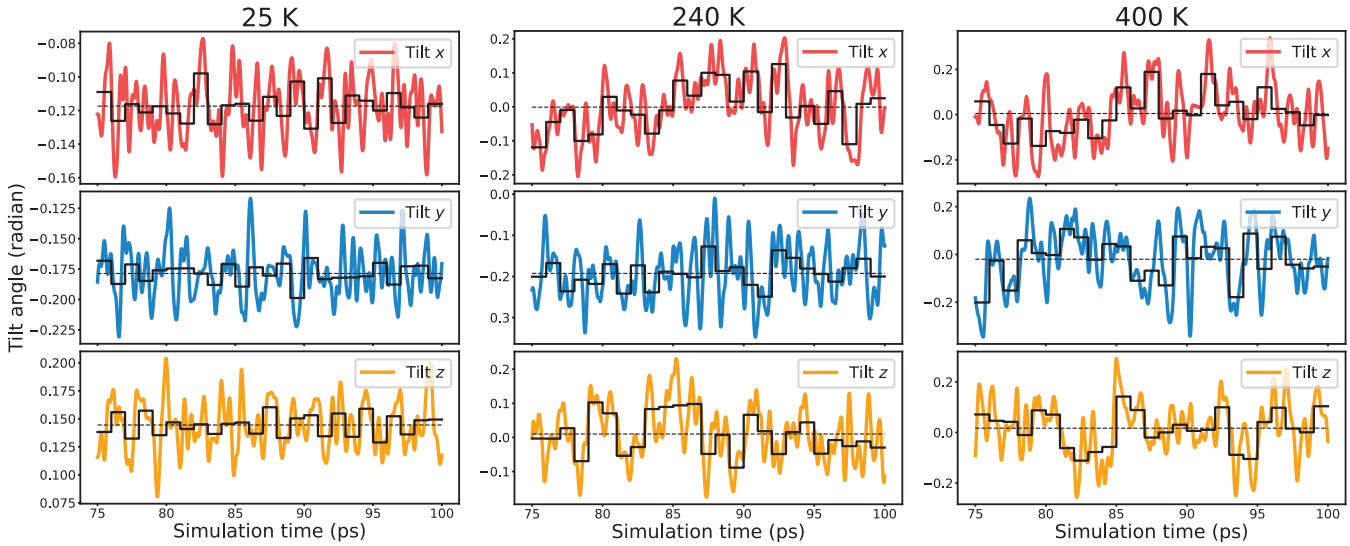

FIG. 3. The time evolution of octahedron tilting of some selected octahedron for bulk 12 × 12 × 12 $CsPbBr_3$, through MPNN-based MD simulations, at temperatures 25 K (orthorhombic, $a^-b^+a^-$), 240 K (tetragonal, $a^0b^+a^0$) and 400 K (cubic, $a^0a^0a^0$). Only the last quarter of the simulation time (from 75 to 100 ps) is used to show the octahedron tilting evolution. The black solid lines correspond to the time average for every 1 ps, and the black dotted lines correspond to the whole time average.

appear when we reduce the number of simulation steps from 100 000 to 50 000 for each temperature during the annealing process and remain like that at the lowest temperature, which is likely caused by the insufficient relaxation at higher temperatures close to the phase transition. Having determined the structural phase transitions of $CsPbBr_3$ and $Cs_2AgBiBr_6$, we further discuss their dynamic behaviors. Figure 3 monitors the time evolution of octahedron tilting in $CsPbBr_3$ as the MD simulation proceeds at different temperatures. At 25 K, the tilting fluctuates mildly around its equilibrium position, with minimal fluctuations (<0.05 radians) due to small thermal motion. While at elevated temperatures 240 K and 400 K, the octahedron tilting exhibits much larger fluctuations of up to 0.2 radians due to strong thermal excitation, which overcome the energy barriers and enable the octahedra to hop dynamically between various energy minima on the PES. More precisely, at a high temperature, the system displays dynamic disorder and hops among variants of $a^-a^-c^+$ tilting configurations [66], and there exist certain low-energy paths for such hops [67], which consequently leads to the $a^0b^+a^0$ tilting in the tetragonal phase (240 K) and the tiltless $a^0a^0a^0$ cubic phase (400 K) on a long-time average.

The dynamic distribution of octahedron tilting is not limited to $CsPbBr_3$. Recent studies suggest that, in perovskites such as $CsSnI_3$ [67] and $CaMnO_3$ [68], the octahedron tilting pattern of tetragonal ($a^0a^0c^+$) and cubic phases ($a^0a^0a^0$) is a time average resulting from the dynamic disorder of octahedron tilts [69], with the system hopping among different but symmetry-equivalent local minima of the PES. Here, with long-time MD simulations, we directly show that the phase transition of perovskites, involving octahedron tilting, is not purely displacive [70], but also exhibits order-disorder characteristics. During the simulation of $Cs_2AgBiBr_6$, we surprisingly observe Frenkel defects [71,72] as Ag ions migrate out of their surrounding Br octahedra to interstitial sites, leaving behind Ag vacancies. To obtain more information about Ag migration, an NPT-MD simulation is performed at ambient temperature (300 K) and zero pressure. The resulting average configuration, as shown in Fig. 4, indicates that Ag ions tend to diffuse to the adjacent sites where normally only Cs is surrounded by Br, resulting in about 90% of Ag out of the

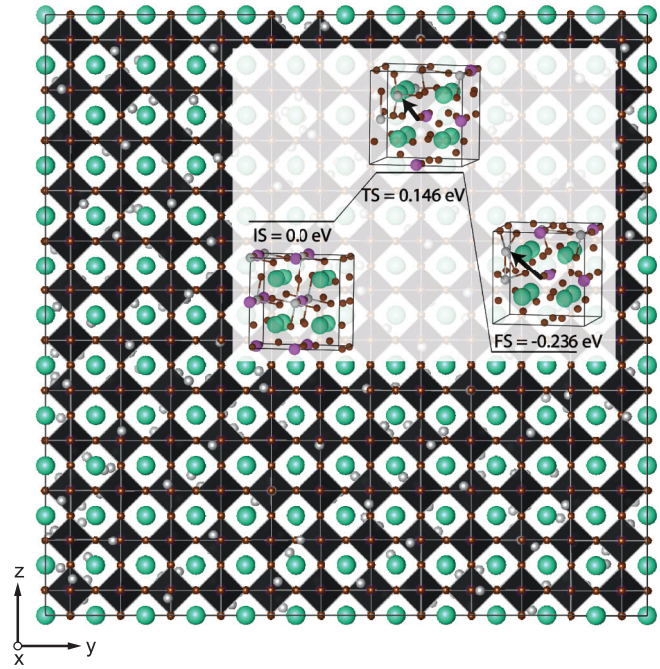

FIG. 4. The average configuration for the NPT-MD simulation of bulk 6 × 6 × 6 $Cs_2AgBiBr_6$ at 300 K, viewed from the x direction, where Cs, Ag, Bi, and Br atoms are in green, gray, pink, and brown color, respectively, and the black octahedra are $BiBr_6$ octahedra. The inset shows the energy changes from initial state (IS) to transition state (TS), and to final state (FS), caused by Ag migration in bulk 1 × 1 × 1 $Cs_2AgBiBr_6$, and only the Ag-Br bonds are drawn.

original $AgBr_6$ octahedron at the end of a 0.4 ns simulation. It has been suggested that the dual-ion-migration of Br and Ag contributes to the degradation of $Cs_2AgBiBr_6$ and lowers its long-term operational stability [73]. In addition, the degree of compositional Ag-Bi disorder can cause defect states and band gap narrowing in $Cs_2AgBiBr_6$ [74]. However, it is remarkable that $Cs_2AgBiBr_6$ retains its double perovskite network with well-ordered Cs, Bi and Br ions, despite significant Ag migration, which indicates that Ag-Bi disorder may not induce significant structural changes in terms of octahedron tilting.

To understand the reason for Ag migration, we conduct DFT calculations by shifting some Ag ion to its neighbor interstitial, in which the linear and quadratic synchronous transit methods [75,76] and the conjugate gradient method [77] are used to locate the transition state, with the $Cs_2AgBiBr_6$ tilting in the $a^0a^0c^-$ pattern. The DFT results are illustrated as the inset in Fig. 4 where the bold black arrows indicate the shifts of the selected Ag ion, revealing that Ag can diffuse easily and favorably to the neighboring interstitial with a small energy barrier of 0.146 eV and negative reaction energy of −0.236 eV. Our results are consistent with previous research based on experiments [73] and DFT calculations [78–80], considering the fact that Ag vacancy defects are quite stable even in Ag-rich compounds, due to their low formation energies [80].

The significance of observing Ag diffusion is twofold: (i) It raises questions about the integrity of $Cs_2AgBiBr_6$ as a perovskite; (ii) It implies that the MPNN model can handle the kinetics of ion migration via direct MD simulations. The MD simulation for ion migration provides insights into the stability of halide perovskites, which are important for their applications as solar cells under ambient conditions. We note that the quantitative results of Ag diffusion in our simulation should be taken with a grain of salt, because the present MPNN model is not specifically trained to treat Ag migration, which can result in special chemical environments that are not well represented by the training data set.

In summary, we have introduced a MPNN-based MD approach to efficiently investigate the temperature-dependent static and dynamic properties of halide perovskites. Tests on $CsPbBr_3$ and $Cs_2AgBiBr_6$ show that this approach can be applied to single-halide perovskites, as well as more complex double halide perovskites. We correctly obtain their phase transition sequences and octahedron tilting patterns, reveal the dynamic nature of octahedron tilting in $CsPbBr_3$, and observe interesting domain walls in $Cs_2AgBiBr_6$, also shedding light on the ion migration in $Cs_2AgBiBr_6$. This study represents a significant advance in the numerical simulation of metal-halide perovskites and will contribute to the development of more stable and efficient solar cells.

This work is financially supported by the National Natural Science Foundation of China (NSFC, Grants No. 11974268 and No. 12111530061). L.L. also acknowledges the support from NSFC (Grant No. 12264012) and Natural Science Foundation of Guangxi (Grant No. ZY22096019).

[1] C. C. Stoumpos and M. G. Kanatzidis, The renaissance of halide perovskites and their evolution as emerging semiconductors, Acc. Chem. Res. **48**, 2791 (2015).

[2] L. N. Quan, F. P. García de Arquer, R. P. Sabatini, and E. H. Sargent, Perovskites for light emission, Adv. Mater. **30**, 1801996 (2018).

[3] F. Heidari Gourji and D. Velauthapillai, A review on Cs-based Pb-free double halide perovskites: From theoretical and experimental studies to doping and applications, Molecules **26**, 2010 (2021).

[4] C. N. Savory, A. Walsh, and D. O. Scanlon, Can Pb-free halide double perovskites support high-efficiency solar cells? ACS Energy Lett. **1**, 949 (2016).

[5] R. Wang, M. Mujahid, Y. Duan, Z.-K. Wang, J. Xue, and Y. Yang, A review of perovskites solar cell stability, Adv. Funct. Mater. **29**, 1808843 (2019).

[6] J.-K. Sun, S. Huang, X.-Z. Liu, Q. Xu, Q.-H. Zhang, W.-J. Jiang, D.-J. Xue, J.-C. Xu, J.-Y. Ma, J. Ding *et al.*, Polar solvent induced lattice distortion of cubic $CsPbI_3$ nanocubes and hierarchical self-assembly into orthorhombic single-crystalline nanowires, J. Am. Chem. Soc. **140**, 11705 (2018).

[7] J. B. Hoffman, A. L. Schleper, and P. V. Kamat, Transformation of sintered $CsPbBr_3$ nanocrystals to cubic $CsPbI_3$ and gradient $CsPbBr_xI_{3-x}$ through halide exchange, J. Am. Chem. Soc. **138**, 8603 (2016).

[8] E. Aktas, N. Rajamanickam, J. Pascual, S. Hu, M. H. Aldamasy, D. Di Girolamo, W. Li, G. Nasti, E. Martínez-Ferrero, A. Wakamiya *et al.*, Challenges and strategies toward long-term stability of lead-free tin-based perovskite solar cells, Commun. Mater. **3**, 104 (2022).

[9] D. Zhang, D. Li, Y. Hu, A. Mei, and H. Han, Degradation pathways in perovskite solar cells and how to meet international standards, Commun. Mater. **3**, 58 (2022).

[10] H. Shahivandi, M. Vaezzadeh, and M. Saeidi, Theory of light-induced degradation in perovskite solar cells, Sol. Energy Mater. Sol. Cells **208**, 110383 (2020).

[11] S. T. Birkhold, J. T. Precht, R. Giridharagopal, G. E. Eperon, L. Schmidt-Mende, and D. S. Ginger, Direct observation and quantitative analysis of mobile Frenkel defects in metal halide perovskites using scanning Kelvin probe microscopy, J. Phys. Chem. C **122**, 12633 (2018).

[12] W. Zhong, D. Vanderbilt, and K. M. Rabe, First-principles theory of ferroelectric phase transitions for perovskites: The case of $BaTiO_3$, Phys. Rev. B **52**, 6301 (1995).

[13] W. Zhong, D. Vanderbilt, and K. M. Rabe, Phase Transitions in $BaTiO_3$ from First Principles, Phys. Rev. Lett. **73**, 1861 (1994).

[14] M. Sepliarsky, Z. Wu, A. Asthagiri, and R. E. Cohen, Atomistic model potential for $PbTiO_3$ and PMN by fitting first principles results, Ferroelectrics **301**, 55 (2004).

[15] H. H. Wu and R. E. Cohen, Electric-field-induced phase transition and electrocaloric effect in PMN-PT, Phys. Rev. B **96**, 054116 (2017).

[16] X. Zeng and R. E. Cohen, Thermo-electromechanical response of a ferroelectric perovskite from molecular dynamics simulations, Appl. Phys. Lett. **99**, 142902 (2011).

[17] J. Klarbring, O. Hellman, I. A. Abrikosov, and S. I. Simak, Anharmonicity and Ultralow Thermal Conductivity in Lead-Free Halide Double Perovskites, Phys. Rev. Lett. **125**, 045701 (2020).

[18] M. A. Carignano, S. A. Aravindh, I. S. Roqan, J. Even, and C. Katan, Critical fluctuations and anharmonicity in lead iodide perovskites from molecular dynamics supercell simulations, J. Phys. Chem. C **121**, 20729 (2017).

[19] A. Cohen, T. M. Brenner, J. Klarbring, R. Sharma, D. H. Fabini, R. Korobko, P. K. Nayak, O. Hellman, and O. Yaffe, Diverging expressions of anharmonicity in halide perovskites, Adv. Mater. **34**, 2107932 (2022).

[20] J. C. Thomas, J. S. Bechtel, A. R. Natarajan, and A. Van der Ven, Machine learning the density functional theory potential energy surface for the inorganic halide perovskite $CsPbBr_3$, Phys. Rev. B **100**, 134101 (2019).

[21] L. Chen, B. Xu, Y. Yang, and L. Bellaiche, Macroscopic and microscopic structures of cesium lead iodide perovskite from atomistic simulations, Adv. Funct. Mater. **30**, 1909496 (2020).

[22] J. Behler, Perspective: Machine learning potentials for atomistic simulations, J. Chem. Phys. **145**, 170901 (2016).

[23] J. Zhang, F. Zhang, D. Wei, L. Liu, X. Liu, D. Fang, G. X. Zhang, X. Chen, and D. Wang, Structural phase transition of monochalcogenides investigated with machine learning, Phys. Rev. B **105**, 094116 (2022).

[24] S. Batzner, A. Musaelian, L. Sun, M. Geiger, J. P. Mailoa, M. Kornbluth, N. Molinari, T. E. Smidt, and B. Kozinsky, E(3)-equivariant graph neural networks for data-efficient and accurate interatomic potentials, Nature Commun. **13**, 2453 (2022).

[25] J. Behler and G. Csányi, Machine learning potentials for extended systems: A perspective, Eur. Phys. J. B **94**, 142 (2021).

[26] T. Mueller, A. Hernandez, and C. Wang, Machine learning for interatomic potential models, J. Chem. Phys. **152**, 050902 (2020).

[27] A. P. Bartók, M. C. Payne, R. Kondor, and G. Csányi, Gaussian Approximation Potentials: The Accuracy of Quantum Mechanics, without the Electrons, Phys. Rev. Lett. **104**, 136403 (2010).

[28] L. Zhang, J. Han, H. Wang, R. Car, and W. E., Deep Potential Molecular Dynamics: A Scalable Model with the Accuracy of Quantum Mechanics, Phys. Rev. Lett. **120**, 143001 (2018).

[29] R. Jinnouchi, J. Lahnsteiner, F. Karsai, G. Kresse, and M. Bokdam, Phase Transitions of Hybrid Perovskites Simulated by Machine-Learning Force Fields Trained on the Fly with Bayesian Inference, Phys. Rev. Lett. **122**, 225701 (2019).

[30] O. T. Unke and M. Meuwly, Physnet: A neural network for predicting energies, forces, dipole moments, and partial charges, J. Chem. Theory Comput. **15**, 3678 (2019).

[31] K. T. Schütt, H. E. Sauceda, P.-J. Kindermans, A. Tkatchenko, and K.-R. Müller, SchNet—a deep learning architecture for molecules and materials, J. Chem. Phys. **148**, 241722 (2018).

[32] J. Gasteiger, S. Giri, J. T. Margraf, and S. Günnemann, Fast and uncertainty-aware directional message passing for non-equilibrium molecules, *Machine Learning for Molecules Workshop, NeurIPS* (2020), arXiv:2011.14115.

[33] J. Gasteiger, J. Groß, and S. Günnemann, Directional message passing for molecular graphs, *International Conference on Learning Representations* (2020), https://openreview.net/forum?id=B1eWbxStPH

[34] D.-X. Zhou, Universality of deep convolutional neural networks, Appl. Comput. Harm. Anal. **48**, 787 (2020).

[35] M. A. Nielsen, A visual proof that neural nets can compute any function, *Neural Networks and Deep Learning* (Determination Press, San Francisco, CA, 2015), Vol. 25, pp. 127–148.

[36] J. Gilmer, S. S. Schoenholz, P. F. Riley, O. Vinyals, and G. E. Dahl, Neural message passing for quantum chemistry, in *International conference on machine learning* (PMLR, 2017), pp. 1263–1272.

[37] A. Kipkorir, J. DuBose, J. Cho, and P. V. Kamat, $CsPbBr_3$–CdS heterostructure: Stabilizing perovskite nanocrystals for photocatalysis, Chem. Sci. **12**, 14815 (2021).

[38] S. Ullah, J. Wang, P. Yang, L. Liu, S.-E. Yang, T. Xia, H. Guo, and Y. Chen, All-inorganic $CsPbBr_3$ perovskite: A promising choice for photovoltaics, Mater. Adv. **2**, 646 (2021).

[39] C. J. Howard, B. J. Kennedy, and P. M. Woodward, Ordered double perovskites – a group-theoretical analysis, Acta Crystallogr B Struct. Sci. **59**, 463 (2003).

[40] L. Schade, A. D. Wright, R. D. Johnson, M. Dollmann, B. Wenger, P. K. Nayak, D. Prabhakaran, L. M. Herz, R. Nicholas, H. J. Snaith *et al.*, Structural and optical properties of $Cs_2AgBiBr_6$ double perovskite, ACS Energy Lett. **4**, 299 (2019).

[41] S. Hirotsu, J. Harada, M. Iizumi, and K. Gesi, Structural phase transitions in $CsPbBr_3$, J. Phys. Soc. Jpn. **37**, 1393 (1974).

[42] M. Rodová, J. Brožek, K. Knížek, and K. Nitsch, Phase transitions in ternary caesium lead bromide, J. Therm. Anal. Calorim. **71**, 667 (2003).

[43] Š. Svirskas, S. Balčiūnas, M. Šimėnas, G. Usevičius, M. Kinka, M. Velička, D. Kubicki, M. E. Castillo, A. Karabanov, V. V. Shvartsman *et al.*, Phase transitions, screening and dielectric response of $CsPbBr_3$, J. Mater. Chem. A **8**, 14015 (2020).

[44] A. Paszke, S. Gross, F. Massa, A. Lerer, J. Bradbury, G. Chanan, T. Killeen, Z. Lin, N. Gimelshein, L. Antiga *et al.*, PyTorch: An imperative style, high-performance deep learning library, in *Proceedings of the 33rd International Conference on Neural Information Processing Systems, NIPS'19* (Curran Associates Inc., 2019), pp. 8026–8037.

[45] K. Schütt, O. Unke, and M. Gastegger, Equivariant message passing for the prediction of tensorial properties and molecular spectra, in *International Conference on Machine Learning* (PMLR, 2021), pp. 9377–9388.

[46] A. P. Thompson, S. J. Plimpton, and W. Mattson, General formulation of pressure and stress tensor for arbitrary many-body interaction potentials under periodic boundary conditions, J. Chem. Phys. **131**, 154107 (2009).

[47] See Supplemental Material at http://link.aps.org/supplemental/10.1103/PhysRevB.108.L020103 for more details about the MPNN method; accuracy of the trained MPNN models; and comparison to bond-valence model. The Supplemental Material also contains Refs. [32,33,42–44,46,60–62].

[48] P. E. Blöchl, Projector augmented-wave method, Phys. Rev. B **50**, 17953 (1994).

[49] G. Kresse and J. Furthmüller, Efficient iterative schemes for *ab initio* total-energy calculations using a plane-wave basis set, Phys. Rev. B **54**, 11169 (1996).

[50] J. Enkovaara, C. Rostgaard, J. J. Mortensen, J. Chen, M. Dułak, L. Ferrighi, J. Gavnholt, C. Glinsvad, V. Haikola, H. Hansen *et al.*, Electronic structure calculations with GPAW: A

real-space implementation of the projector augmented-wave method, J. Phys.: Condens. Matter **22**, 253202 (2010).

[51] A. H. Larsen, J. J. Mortensen, J. Blomqvist, I. E. Castelli, R. Christensen, M. Dułak, J. Friis, M. N. Groves, B. Hammer, C. Hargus *et al.*, The atomic simulation environment—a Python library for working with atoms, J. Phys.: Condens. Matter **29**, 273002 (2017).

[52] J. P. Perdew, K. Burke, and M. Ernzerhof, Generalized Gradient Approximation Made Simple, Phys. Rev. Lett. **77**, 3865 (1996).

[53] S. Melchionna, G. Ciccotti, and B. Lee Holian, Hoover NPT dynamics for systems varying in shape and size, Mol. Phys. **78**, 533 (1993).

[54] H. A. Posch, W. G. Hoover, and F. J. Vesely, Canonical dynamics of the Nosé oscillator: Stability, order, and chaos, Phys. Rev. A **33**, 4253 (1986).

[55] C. J. Howard and H. T. Stokes, Group-theoretical analysis of octahedral tilting in perovskites, Acta Crystallogr B Struct. Sci. **54**, 782 (1998).

[56] A. M. Glazer, The classification of tilted octahedra in perovskites, Acta Crystallogr B Struct. Crystallogr Cryst. Chem. **28**, 3384 (1972).

[57] E. L. da Silva, J. M. Skelton, S. C. Parker, and A. Walsh, Phase stability and transformations in the halide perovskite $CsSnI_3$, Phys. Rev. B **91**, 144107 (2015).

[58] S. F. Yuk, K. C. Pitike, S. M. Nakhmanson, M. Eisenbach, Y. W. Li, and V. R. Cooper, Towards an accurate description of perovskite ferroelectrics: Exchange and correlation effects, Sci. Rep. **7**, 43482 (2017).

[59] A. Paul, J. Sun, J. P. Perdew, and U. V. Waghmare, Accuracy of first-principles interatomic interactions and predictions of ferroelectric phase transitions in perovskite oxides: Energy functional and effective Hamiltonian, Phys. Rev. B **95**, 054111 (2017).

[60] Q. You, S. Gu, and X. Gou, The highly accurate interatomic potential of $CsPbBr_3$ perovskite with temperature dependence on the structure and thermal properties, Materials **16**, 2043 (2023).

[61] I. D. Brown, Recent developments in the methods and applications of the bond valence model, Chem. Rev. **109**, 6858 (2009).

[62] E. Levi, D. Aurbach, and C. Gatti, A revisit of the bond valence model makes it universal, Phys. Chem. Chem. Phys. **22**, 13839 (2020).

[63] D. Malyshkin, V. Sereda, I. Ivanov, M. Mazurin, A. Sednev-Lugovets, D. Tsvetkov, and A. Zuev, New phase transition in $CsPbBr_3$, Mater. Lett. **278**, 128458 (2020).

[64] N. Xie, J. Zhang, S. Raza, N. Zhang, X. Chen, and D. Wang, Generation of low-symmetry perovskite structures for *ab initio* computation, J. Phys.: Condens. Matter **32**, 315901 (2020).

[65] E. T. McClure, M. R. Ball, W. Windl, and P. M. Woodward, Cs_2AgBiX_6 (X = Br, Cl): new visible light absorbing, lead-free halide perovskite semiconductors, Chem. Mater. **28**, 1348 (2016).

[66] J. S. Bechtel and A. Van der Ven, Octahedral tilting instabilities in inorganic halide perovskites, Phys. Rev. Mater. **2**, 025401 (2018).

[67] J. Klarbring, Low-energy paths for octahedral tilting in inorganic halide perovskites, Phys. Rev. B **99**, 104105 (2019).

[68] J. Klarbring and S. I. Simak, Nature of the octahedral tilting phase transitions in perovskites: A case study of $CaMnO_3$, Phys. Rev. B **97**, 024108 (2018).

[69] F. Bertolotti, L. Protesescu, M. V. Kovalenko, S. Yakunin, A. Cervellino, S. J. Billinge, M. W. Terban, J. S. Pedersen, N. Masciocchi, and A. Guagliardi, Coherent nanotwins and dynamic disorder in cesium lead halide perovskite nanocrystals, ACS Nano **11**, 3819 (2017).

[70] A. L. Goodwin, S. A. T. Redfern, M. T. Dove, D. A. Keen, and M. G. Tucker, Ferroelectric nanoscale domains and the 905 K phase transition in $SrSnO_3$: A neutron total-scattering study, Phys. Rev. B **76**, 174114 (2007).

[71] E. Kotomin and V. Kuzovkov, Phenomenological kinetics of Frenkel defect recombination and accumulation in ionic solids, Rep. Prog. Phys. **55**, 2079 (1992).

[72] A. Lushchik, C. Lushchik, K. Schwartz, F. Savikhin, E. Shablonin, A. Shugai, and E. Vasil'Chenko, Creation and clustering of Frenkel defects at high density of electronic excitations in wide-gap materials, Nucl. Instrum. Meth. Phys. Res. B **277**, 40 (2012).

[73] M. Ghasemi, L. Zhang, J.-H. Yun, M. Hao, D. He, P. Chen, Y. Bai, T. Lin, M. Xiao, A. Du *et al.*, Dual-ion-diffusion induced degradation in lead-free $Cs_2AgBiBr_6$ double perovskite solar cells, Adv. Funct. Mater. **30**, 2002342 (2020).

[74] F. Ji, J. Klarbring, F. Wang, W. Ning, L. Wang, C. Yin, J. S. M. Figueroa, C. K. Christensen, M. Etter, T. Ederth *et al.*, Lead-free halide double perovskite $Cs_2AgBiBr_6$ with decreased band gap, Angew. Chem. **132**, 15303 (2020).

[75] T. A. Halgren and W. N. Lipscomb, The synchronous-transit method for determining reaction pathways and locating molecular transition states, Chem. Phys. Lett. **49**, 225 (1977).

[76] N. Govind, M. Petersen, G. Fitzgerald, D. King-Smith, and J. Andzelm, A generalized synchronous transit method for transition state location, Comput. Mater. Sci. **28**, 250 (2003).

[77] J. L. Nazareth, Conjugate gradient method, WIREs Comp. Stat. **1**, 348 (2009).

[78] Z. Xiao, W. Meng, J. Wang, and Y. Yan, Thermodynamic stability and defect chemistry of bismuth-based lead-free double perovskites, ChemSusChem **9**, 2628 (2016).

[79] H. Chen, C.-R. Zhang, Z.-J. Liu, J.-J. Gong, W. Wang, Y.-Z. Wu, and H.-S. Chen, Vacancy defects on optoelectronic properties of double perovskite $Cs_2AgBiBr_6$, Mater. Sci. Semicond. Proc. **123**, 105541 (2021).

[80] T. Li, X. Zhao, D. Yang, M.-H. Du, and L. Zhang, Intrinsic Defect Properties in Halide Double Perovskites for Optoelectronic Applications, Phys. Rev. Appl. **10**, 041001(R) (2018).